

Capillary adhesion between elastic solids with randomly rough surfaces

B N J Persson

IFF, FZ-Jülich, 52425 Jülich, Germany

Received 3 April 2008, in final form 22 May 2008

Published 26 June 2008

Online at stacks.iop.org/JPhysCM/20/315007

Abstract

I study how the contact area and the work of adhesion between two elastic solids with randomly rough surfaces depend on the relative humidity. The surfaces are assumed to be hydrophilic, and capillary bridges form at the interface between the solids. For elastically hard solids with relatively smooth surfaces, the area of real contact and therefore also the sliding friction are maximal when there is just enough liquid to fill out the interfacial space between the solids, which typically occurs for $d_K \approx 3h_{\text{rms}}$, where d_K is the height of the capillary bridge and h_{rms} the root-mean-square roughness of the (combined) surface roughness profile. For elastically soft solids, the area of real contact is maximal for very low humidity (i.e. small d_K), where the capillary bridges are able to pull the solids into nearly complete contact. In both cases, the work of adhesion is maximal (and equal to $2\gamma \cos \theta$, where γ is the liquid surface tension and θ the liquid–solid contact angle) when $d_K \gg h_{\text{rms}}$, corresponding to high relative humidity.

(Some figures in this article are in colour only in the electronic version)

1. Introduction

When two solids are in close contact capillary bridges may form at the interface, either as a result of liquid-like contamination layers (e.g. organic contamination from the normal atmosphere) or water condensation in a humid atmosphere, or intentionally added thin fluid layers, e.g. thin lubrication films. For wetting liquids strong negative pressure will prevail in (short) capillary bridges, which will act as an effective relative long-ranged attraction between the solids [1]. In many cases, in particular for hard solids and with rough surfaces, the contribution to the wall–wall attraction from capillary bridges may be much larger than the contribution from the direct wall–wall interaction, e.g. the van der Waals interaction between the solids. The capillary bridge mediated wall–wall interaction has a huge number of important applications, e.g. for granular materials [2], insect or tree frog adhesion [3–5], head/disk systems [6] and microelectromechanical systems (MEMS) [7], where they may trigger permanent adhesion and device failure.

The influence of capillary bridges on adhesion is well known to all of us. Thus, it is possible to build sand castles from humid or slightly wet sand but not from dry sand or sand flooded with water. Similarly, it is well known that very flat surfaces, such as those of gauge blocks (steel blocks with the roughness amplitude of the order of ~ 25 nm when measured

over a macroscopic area, e.g. 50 cm^2), adhere with strong forces resulting from capillary bridges formed from organic contamination or water. Thus it may easily be shown that the force to separate two gauge blocks may strongly increase if one exposes the surfaces to (humid) breath (for strong adhesion, the fluid layer (organic or water) should be at least several times larger than the surface root-mean-square roughness amplitude, i.e. in the present case of the order of 100 nm, or more; see below). Finally, the fact that a fly can walk on a vertical glass window is due to capillary bridges formed at the tip of many thin hair-like fibers, which cover the attachment organs of the fly; see figure 1. Without the fluid (injected via channels in the fibers) adhesion would probably be impossible to most surfaces because too much elastic energy is necessary to bend the tips of the fibers into atomic contact with the rough substrate, which is necessary for strong adhesion without fluids. (The tips of the hair covering the attachment pads of some lizards (e.g. geckos) and most spiders are much thinner than those of a fly, and can easily be bent to make atomic contact even to very rough surfaces; in these cases no liquid is injected by the animal into the contact area.)

Capillary adhesion between solids with randomly rough surfaces has been studied so far mainly using the Greenwood–Williamson contact mechanics theory [8]. In this theory the asperities on the rough surfaces are approximated by spherical cups and the long-range elastic coupling is neglected. It has

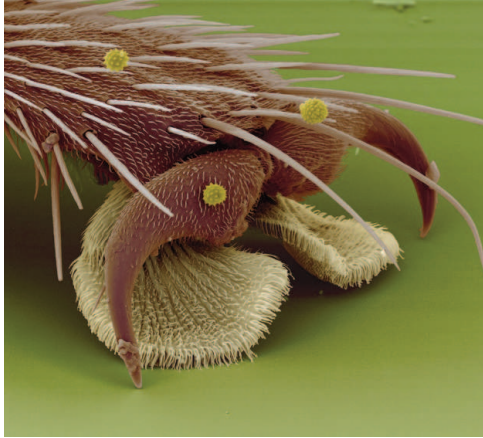


Figure 1. The attachment organ of a fly. At the tips of the hairs on the attachment pads occur thin elastic plates. The fly injects a liquid into the space between the plate and the substrate. The resulting capillary bridge makes it possible for the fly to adhere to surfaces with large roughness. To very rough surfaces, the fly can also ‘adhere’ using the claws on the legs. Reproduced with permission from S Gorb and J Berger (Max Planck Institute, Germany).

recently been shown [9, 10] that for surfaces with roughness on many length scales the GW theory (and other asperity contact theories such as the theory of Bush *et al* [11]) fail qualitatively to describe e.g. the area of real contact and the interfacial separation as a function of the load.

When two elastic solids with rough surfaces are squeezed together, the solids will in general not make contact everywhere in the apparent contact area, but only at a distribution of asperity contact spots [12–15]. The separation $u(\mathbf{x})$ between the surfaces will vary in a nearly random way with the lateral coordinates $\mathbf{x} = (x, y)$ in the apparent contact area. When the applied squeezing pressure increases, the average surface separation $\bar{u} = \langle u(\mathbf{x}) \rangle$ will decrease, but in most situations it is not possible to squeeze the solids into perfect contact corresponding to $\bar{u} = 0$. In thermal equilibrium, capillary bridges are formed at the wall–wall interface in those regions where the separation $u(\mathbf{x})$ is below the Kelvin length d_K , which depends on the relative humidity and on the liquid contact angles with the solid walls.

Here I will present a general theory of capillary adhesion between elastic solids with randomly rough surfaces. The study is based on a recently developed theory for the (average) surface separation \bar{u} as a function of the squeezing pressure p . The theory shows that for randomly rough surfaces at low squeezing pressures $p \sim \exp(-\alpha\bar{u}/h_{\text{rms}})$, where $\alpha \approx 2$ depends (weakly) on the nature of the surface roughness but is independent of p , in good agreement with experiments [16]. The GW contact mechanics theory (and the more accurate theory of Bush *et al*) instead predicts $p \sim \bar{u}^{-a} \exp[-b(\bar{u}/h_{\text{rms}})^2]$ (where a and b are positive numbers), in strong disagreement with numerical simulations [17–19] and experiment [16].

The theory presented below is based on solid and fluid continuum mechanics. Thus it cannot be strictly applied when the Kelvin distance d_K becomes of the order of the molecular size, i.e. smaller than ~ 1 nm. The limiting case

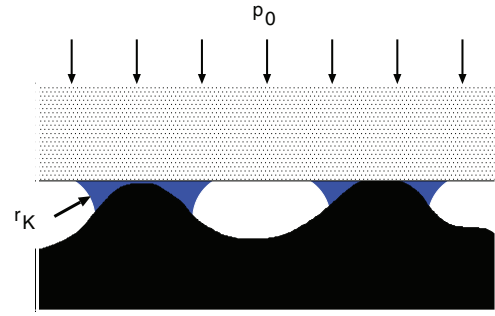


Figure 2. Capillary bridges formed at two asperity contact areas. At thermal equilibrium, the radius of curvature of the capillary bridge r_K is given by the Kelvin radius. The capillary bridges will exert an attractive force F_a on the block. The sum of the capillary force F_a and the external load $F_0 = p_0 A_0$ (where A_0 is the nominal surface area) must equal the repulsive force arising from the area of real contact between the solids.

of molecular thin fluid films must be treated using atomistic methods, e.g. molecular dynamics (see, e.g., [20, 21]).

2. Theory

Consider the frictionless contact between two elastic solids with the Young’s elastic modulus E_1 and E_2 and the Poisson ratios ν_1 and ν_2 . Assume that the solid surfaces have the height profiles $h_1(\mathbf{x})$ and $h_2(\mathbf{x})$, respectively. The elastic contact mechanics for the solids is equivalent to those of a rigid substrate with the height profile $h(\mathbf{x}) = h_1(\mathbf{x}) + h_2(\mathbf{x})$ and a second elastic solid with a flat surface and with the Young’s modulus E and the Poisson ratio ν chosen so that [22]

$$\frac{1 - \nu^2}{E} = \frac{1 - \nu_1^2}{E_1} + \frac{1 - \nu_2^2}{E_2}. \quad (1)$$

Consider an elastic block with a flat surface in contact with a hard rough substrate. We consider humid conditions (vapor pressure P_v) and assume that the liquid wets the surfaces. In this case, in the asperity contact regions liquid capillary bridges will form (see figure 2), where the meniscus radius r_K is given by the Kelvin equation

$$r_K = -\frac{\gamma v_0}{k_B T \ln(P_v/P_{\text{sat}})}, \quad (2)$$

where v_0 is the molecular volume in the liquid. Thus, the thickness of the liquid film is given by

$$d_K = r_K(\cos \theta_1 + \cos \theta_2), \quad (3)$$

where θ_1 and θ_2 are the liquid contact angles on the two solid surfaces.

For water at $T = 300$ K, $\gamma = 0.073$ J m⁻² and $v_0 \approx 3 \times 10^{-29}$ m³ so that

$$r_K \approx -\frac{0.53 \text{ nm}}{\ln(P_v/P_{\text{sat}})}.$$

Thus, if water wets the surfaces (i.e. $\theta_1 = \theta_2 = 0$) the thickness of the liquid film is given by the Kelvin length

$$d_K \approx -\frac{1.06 \text{ nm}}{\ln(P_v/P_{\text{sat}})}. \quad (4)$$

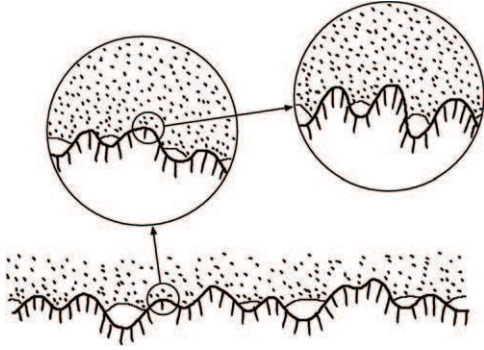


Figure 3. A rubber block (dotted area) in adhesive contact with a hard rough substrate (dashed area). The substrate has roughness on many different length scales and the rubber makes partial contact with the substrate on all length scales. When a contact area is studied at low magnification it appears as if complete contact occurs, but when the magnification is increased it is observed that in reality only partial contact occurs.

We now use the contact mechanics formalism developed elsewhere [17, 23–26], where the system is studied at different magnifications ζ ; see figure 3. When the system is studied at the magnification ζ it appears as if the contact area (projected on the xy -plane) equals $A(\zeta)$, but when the magnification increases it is observed that the contact is incomplete, and the surfaces in the apparent contact area $A(\zeta)$ are in fact separated by the average distance $\bar{u}(\zeta)$, see figure 4. Let $u_1(\zeta)$ be the (average) height separating the surfaces which appear to come into contact when the magnification decreases from ζ to $\zeta - \Delta\zeta$, where $\Delta\zeta$ is a small (infinitesimal) change in the magnification. $u_1(\zeta)$ is a monotonically decreasing function of ζ , and can be calculated from $\bar{u}(\zeta)$ and $A(\zeta)$ using (see [17])

$$u_1(\zeta) = \bar{u}(\zeta) + \bar{u}'(\zeta)A(\zeta)/A'(\zeta). \quad (5)$$

We assume that liquid occurs in the apparent contact areas when the separation $u_1(\zeta)$ is smaller than (or equal to) the Kelvin distance d_K . Assume that this occurs for the magnification $\zeta = \zeta_K$ so that

$$u_1(\zeta_K, p_0) = d_K, \quad (6)$$

where we have indicated that the separation u_1 depends on the nominal pressure p_0 . In the liquid bridge is a negative pressure $p = -p_K$ with $p_K = 2\gamma/d_K$. The liquid occupies the (projected) surface area $\Delta A = A(\zeta_K) - A(\zeta_1)$, where $A(\zeta_1)$ is the area of real contact observed at the highest magnification ζ_1 . Thus the attractive force

$$F_a = p_K \Delta A = \frac{2\gamma}{d_K} [A(\zeta_K) - A(\zeta_1)]. \quad (7)$$

We define $p_a = F_a/A_0$. We will calculate $A(\zeta)$ by using a mean-field type of approximation, where instead of including the non-uniform distribution of capillary forces acting at the block–substrate interface we assume that the effective squeezing pressure is $p = p_0 + p_a$, where $p_0 = F_0/A_0$ is the applied squeezing pressure (which is negative during pull-off) (see figure 2 and also section 5).

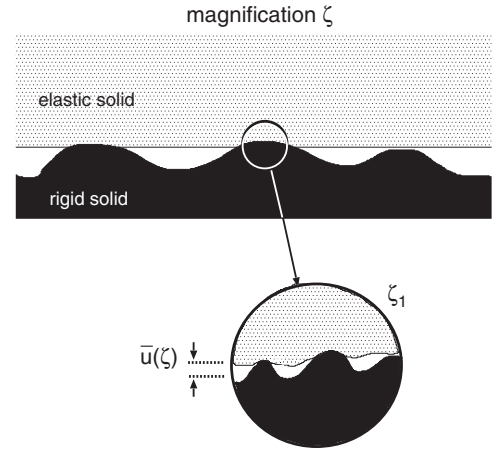


Figure 4. An asperity contact region observed at the magnification ζ . It appears that complete contact occurs in the asperity contact region, but upon increasing the magnification to the highest resolution (magnification ζ_1) it is observed that the solids are separated by the (average) distance $\bar{u}(\zeta)$.

Let us apply a pull-off force $F_0 = -F_{\text{pull}}$ to the block. We define the work of adhesion per unit area as

$$w = \frac{1}{A_0} \int_{u_0}^{\infty} du F_{\text{pull}}(u) = \int_{u_0}^{\infty} du [p_a - p(u)]. \quad (8)$$

$p(u)$ is the repulsive pressure from the substrate at the separation $u = \bar{u}$ between the average substrate surface plane and the average position of the bottom surface of the block. u_0 is the equilibrium separation when $F_{\text{pull}} = 0$, i.e., $p(u_0) = p_a$.

Let us now study the limiting case when the space between the solids is filled with liquid, i.e. no dry area. We also assume that the area of real contact $A(\zeta_1)$ is negligible compared to the nominal contact area A_0 . In this case the attractive pressure $p_a = 2\gamma/d_K$ must be balanced by the repulsive asperity contact pressure, which for separation $u \gtrsim h_{\text{rms}}$ is given by

$$p(u) = \beta E^* e^{-\alpha \bar{u}/h_{\text{rms}}} \quad (9)$$

where α and β are numbers which depend on the surface roughness but which are independent of p and of the elastic properties of the solids [18]. Thus

$$\frac{2\gamma}{d_K} = \beta E^* e^{-\alpha u_0/h_{\text{rms}}}, \quad (10)$$

or

$$u_0 = \frac{h_{\text{rms}}}{\alpha} \log \frac{\beta E^* d_K}{2\gamma}. \quad (11)$$

Since the capillary pressure is $p_a = 2\gamma/d_K$ for $u < d_K$ and zero otherwise, we get work of adhesion

$$\begin{aligned} w &= \int_{u_0}^{\infty} du [p_a - p(u)] \\ &= \frac{2\gamma}{d_K} (d_K - u_0) - \frac{\beta E^* h_{\text{rms}}}{\alpha} e^{-\alpha u_0/h_{\text{rms}}}. \end{aligned} \quad (12)$$

Using (11) this gives

$$w = 2\gamma \left[1 - \frac{h_{\text{rms}}}{\alpha d_K} \log \left(\frac{e\beta E^* d_K}{2\gamma} \right) \right]. \quad (13)$$

For self-affine fractal surfaces we have [18] $\alpha \approx 2$ and $\beta \approx 0.4q_0h_{\text{rms}}$, giving

$$w \approx 2\gamma \left[1 - \frac{h_{\text{rms}}}{2d_K} \log \left(\frac{q_0 h_{\text{rms}} E^* d_K}{2\gamma} \right) \right], \quad (14)$$

where q_0 is the roll-off (or cut-off) wavevector of the surface roughness power spectrum.

The analysis above has assumed that thermal equilibrium occurs at any moment in time during pull-off, which requires a static or slowly propagating debonding crack. In this case liquid will condense or evaporate at the interface in such a way as to always maintain the Kelvin radius $r_K = d_K/2$ for the radius of curvature of the liquid meniscus. However, during fast pull-off negligible condensation or evaporation occurs, and the fluid volume at the interface, rather than the Kelvin radius, will be constant during pull-off. If $A(u)$ is the area covered by liquid when the average surface separation is u , then volume conservation requires $A_0 u_0 = A(u)u$ or $A(u)/A_0 = u_0/u$. In this case

$$\int_{u_0}^{\infty} du p_a(u) = \int_{u_0}^{\infty} du \frac{2\gamma}{u} \frac{A(u)}{A_0} = 2\gamma.$$

When thermal equilibrium occurs during pull-off the same integral becomes $2\gamma(1 - u_0/d_K)$. Thus, when $u_0/d_K \ll 1$, the whole interface is filled with fluid, and the adiabatic pull-off (constant meniscus radius) and fast pull-off (constant fluid volume) give nearly the same result for the work of adhesion, assuming that one may neglect viscous energy dissipation in the fluid during the fast pull-off (which is responsible for the suction-cup type of effective adhesion).

In general, for most solids with covalent, ionic or metallic bonds $E \approx 10^{11}$ Pa, and in the normal atmosphere (where d_K is of nanometer size) capillary adhesion will only be observed if h_{rms} is at most a few nanometers. In fact, assuming that (14) is valid we get $w = 0$ if

$$d_K < d_c = \frac{h_{\text{rms}}}{2} \log \left(\frac{q_0 h_{\text{rms}} E^* d_c}{2\gamma} \right). \quad (15)$$

Since d_c only depends logarithmically on the parameters q_0 , E^* and γ , the critical Kelvin distance (or humidity), below which the adhesion is very small, depends weakly on these parameters. For example, if $h_{\text{rms}} \approx 2$ nm, and with the roll-off wavevector $q_0 \sim 10^7 \text{ m}^{-1}$ (as for the lower curve in figure 5), we get $\log(q_0 h_{\text{rms}} E^* d_K/2\gamma) \approx 5$ so that $d_c \approx 5$ nm, corresponding to $\sim 80\%$ relative humidity.

As another application of (14), let us study the case where $E^* = 1$ GPa (as typical for glassy polymers) in contact with a hard rough substrate with $h_{\text{rms}} = 1 \mu\text{m}$ and $q_0 = 10^4 \text{ m}^{-1}$. Using $\gamma \approx 0.1 \text{ J m}^{-2}$ (14) gives that $w > 0$ only if $d_K > 10 \mu\text{m}$. More generally, (14) shows that capillary adhesion will only manifest itself as long as the the Kelvin length d_K is (at least) a few times the root-mean-square amplitude of the (combined) substrate roughness profile. This statement only holds for elastically hard enough solids—for very soft solids the negative capillary pressure can pull the solids into close contact, in which case (14) is no longer valid; see section 3.2.

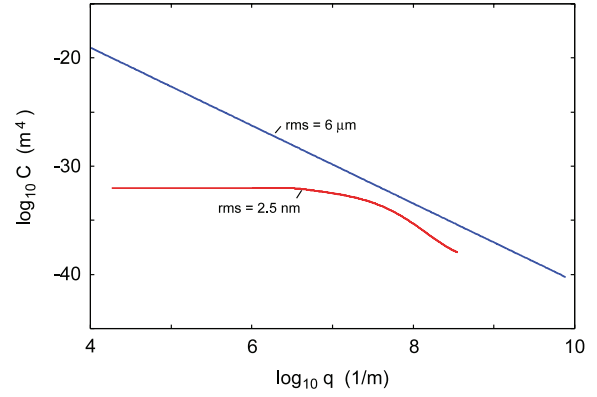


Figure 5. The surface roughness power spectrum of two surfaces. The surface with the root-mean-square (rms) roughness $6 \mu\text{m}$ is a self-affine fractal with the fractal dimension $D_f = 2.2$. The other surface has the rms roughness 2.4 nm and is assumed to be randomly rough.

3. Numerical results

We will apply the theory to two cases, namely the contact between elastically hard solids, e.g. silicon as relevant for microelectromechanical systems (MEMSs), and elastically soft systems such as rubber or biological adhesive pads. For the case of hard solids we will assume that the (combined) rough surface has the surface roughness power spectrum $C(q)$ shown in figure 5, bottom curve. This power spectrum was obtained from the surface topography, $h(\mathbf{x})$, measured [27] for a polysilicon surface, using [28]

$$C(q) = \frac{1}{(2\pi)^2} \int d^2x \langle h(\mathbf{x})h(\mathbf{0}) \rangle e^{-iq \cdot \mathbf{x}}.$$

The root-mean-square (rms) roughness of this surface is 2.4 nm . For the case of elastically soft solids we will assume that the combined surface has the power spectrum shown in figure 5, top curve. This is the power spectrum of a self-affine fractal surface with the rms roughness $6 \mu\text{m}$ and the fractal dimension $D_f = 2.2$.

3.1. Elastically hard solids

In figure 6 we show the stress as a function of the (average) distance between the surfaces, \bar{u} , during separation for several different relative humidities (RHs), 0.95, 0.925, 0.9 and 0.875. The elastic solid has the Young's modulus $E = 82 \text{ GPa}$ and the Poisson ratio $\nu = 0.22$. The area under the curves in figure 6 determines the work of adhesion, which is shown in figure 7. The numerical results in figure 7 are in relatively good agreement with the (approximate) analytical result (14) (curve denoted by 'approx' in figure 7).

In figure 8 we compare the work of adhesion, as a function of the relative humidity, with the experimental data of DelRio *et al* [29, 30], obtained from microcantilever experiments. The circles are experimental data and the squares calculated results (from figure 7). The experimental system is for polysilicon surfaces with the combined surface having the root-mean-square (rms) roughness [29] $\approx 2.3 \text{ nm}$, while in the calculation

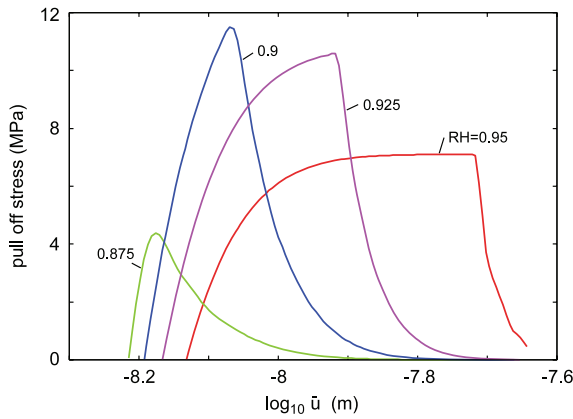


Figure 6. The stress as a function of the logarithm of the (average) separation \bar{u} during separation. The area under the curves determines the work of adhesion. For a hard surface with the root-mean-square roughness $h_{\text{rms}} = 2.4$ nm in contact with an elastic solid (with the Young's modulus $E = 82$ GPa and Poisson ratio $\nu = 0.22$) with a flat surface. Results are shown for the relative humidities (RHs) 0.95, 0.925, 0.9, 0.875.

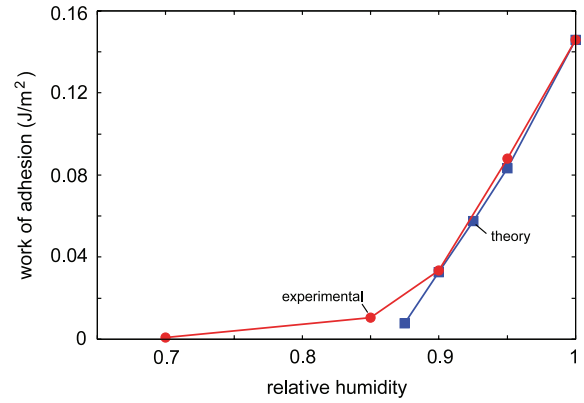


Figure 8. The work of adhesion as a function of the relative humidity. The circles are experimental data (from [29]) and the squares calculated results. In the calculation we have assumed a hard surface with the root-mean-square roughness $h_{\text{rms}} = 2.4$ nm in contact with an elastic solid (with the Young's modulus $E = 82$ GPa and Poisson ratio $\nu = 0.22$) with a flat surface. The square data points are the calculated results for the relative humidities (RHs) 0.95, 0.925, 0.9, 0.875.

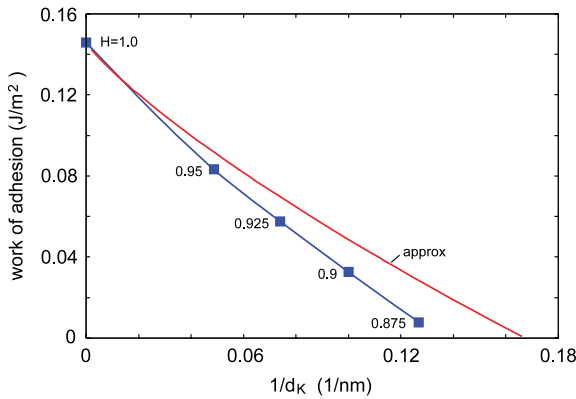


Figure 7. The work of adhesion as a function of the inverse of the height d_K of the capillary bridges. For a hard surface with the root-mean-square roughness $h_{\text{rms}} = 2.4$ nm in contact with an elastic solid (with the Young's modulus $E = 82$ GPa and Poisson ratio $\nu = 0.22$) with a flat surface. The square data points are the calculated results for the relative humidities (RHs) 0.95, 0.925, 0.9, 0.875, and the solid line a fit to the data. The line denoted by 'approx' is given by (13) with $\alpha = 1.87$ as calculated [17] from the measured surface roughness power spectrum.

we have assumed the same system as above where the rough surface has the rms roughness $h_{\text{rms}} \approx 2.4$ nm.

In figure 9 I show the calculated work of adhesion as a function of the relative humidity. In the calculation I have assumed hard surfaces with the root-mean-square roughness $h_{\text{rms}} = 2.4$ (from figure 8) and 3 nm. The power spectrum of the second surface was obtained from the original power spectrum (bottom curve in figure 5) by scaling it with a factor of $(3/2.4)^2$. The slope of the rms = 3 nm line is about 25% larger than for the rms = 2.4 nm curve. This is just the ratio between the two rms values and agrees with the prediction of the (simplified) theory, equation (14), which shows that the slope of the work of adhesion curve scales approximately linearly with the rms value. This prediction is very different

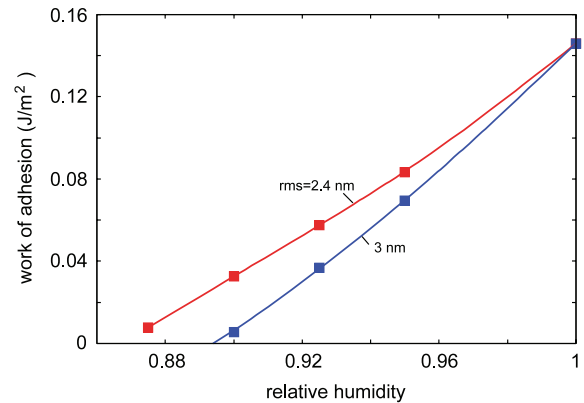


Figure 9. The work of adhesion as a function of the relative humidity. In the calculation we have assumed hard surfaces with the root-mean-square roughness $h_{\text{rms}} = 2.4$ and 3 nm in contact with an elastic solid (with the Young's modulus $E = 82$ GPa and Poisson ratio $\nu = 0.22$) with a flat surface. The square data points are the calculated results and the lines smoothing cubic splines.

from the GW theory prediction, which indicates much larger change in the work of adhesion.

In the present case the theory predicts that the work of adhesion per unit area, w , vanishes for $\text{RH} < 0.87$ (see figure 8) or, equivalently, for the capillary heights $d_K < 8$ nm (see figure 7). In the experiment w is indeed very small for $\text{RH} < 0.87$ but not zero (see figure 8), and we attribute this difference between theory and experiment to two different effects.

(1) *Finite size effect.* The theory is for an infinite system while the experimental system is finite, and in the present case in fact quite small (the crack-tip process zone has a total area of only $\sim 100 \mu\text{m}^2$; see [31]). A finite pull-off force due to capillary bridges will in reality always occur, even in the limit of very low RH, where (for a small system and solids with high elastic modulus) a single asperity (or just a few asperities)

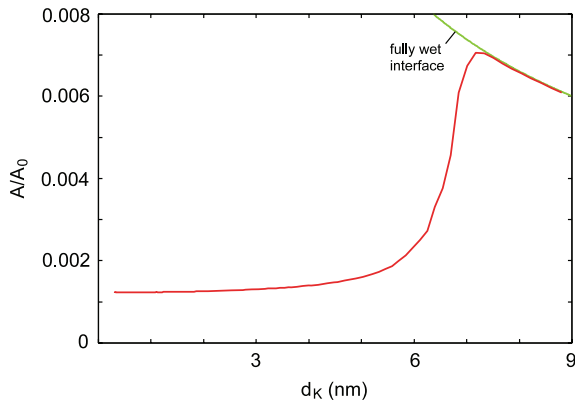


Figure 10. The area of real contact as a function of the Kelvin capillary width d_K . For a hard surface with the root-mean-square roughness $h_{\text{rms}} = 2.4$ nm in contact with elastic solids with the Poisson ratio $\nu = 0.22$ and the Young modulus $E = 82$ GPa. The (nominal) squeezing pressure $p = 4$ MPa.

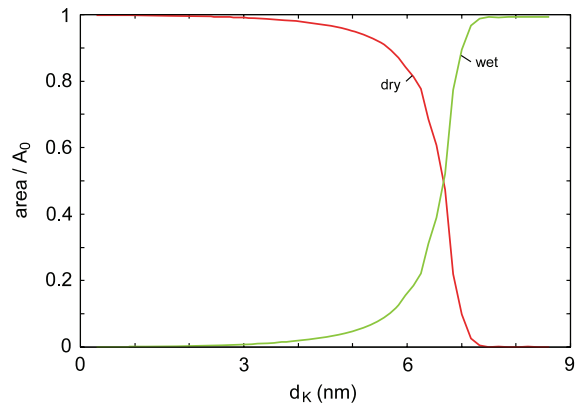


Figure 11. The dry and wet area as a function of the Kelvin capillary width d_K . For a hard surface with the root-mean-square roughness $h_{\text{rms}} = 2.4$ nm in contact with elastic solids with the Poisson ratio $\nu = 0.22$ and the Young modulus $E = 82$ GPa. The (nominal) squeezing pressure $p = 4$ MPa.

may be in contact—in this case a (small) capillary bridge can form at the asperity, giving a non-zero pull-off force. For a finite-sized system this will result in a non-zero work per unit area, w , to separate the solids (which may be non-negligible for micro- and nano-sized systems), but in the thermodynamic limit (infinite-sized system, as assumed in the theory) w would of course vanish. The small contact between small, elastically hard, solids also implies that there will be large fluctuations in the pull-off force between different realizations of the same system. This has indeed been observed by Zwol *et al* [32], who found that the pull-off force (at low relative humidity) varied by a factor of ~ 2 (or more), when the same micro-sized object was brought into contact with the same substrate surface at different locations (see also section 5).

(2) *Van der Waals interaction.* One can easily show that the long-ranged van der Waals interaction will always give a non-zero work of adhesion. The reason for this is that the (repulsive) contribution to the wall–wall interaction from the elastic deformation of asperities decays as $\sim \exp(-\alpha\bar{u}/h_{\text{rms}})$ (or faster, if finite size effects are taken into account) with increasing wall separation \bar{u} , while the (attractive) van der Waals interaction decays slower as $\sim 1/\bar{u}^3$ and the total interaction will always be attractive for large enough separation \bar{u} . With only the capillary bridges the wall–wall interaction is predicted to be repulsive (for all wall–wall separations) at low relative humidity. Combining the van der Waals interaction and the capillary contribution will give a non-zero work of adhesion even for small relative humidity, which still depends on the relative humidity. I plan to study this in more detail in the future.

It is interesting to compare (14) with the predictions of the Greenwood–Williamson (GW) theory of contact mechanics. As pointed out before, this theory fails qualitatively when roughness occurs on many length scales, and DelRio *et al* found that the GW theory strongly underestimate the work of adhesion. The main reason for this failure is not the asperity approximation (which, however, also is a severe approximation in the present case) but the neglect of elastic coupling between the contact regions.

The separation of two solids usually occurs via interfacial crack propagation, which depends on the work of adhesion. However, the sliding friction is determined mainly by the area of real contact. In figure 10 we show the area of real contact as a function of the Kelvin length d_K . The (nominal) squeezing pressure is $p = 4$ MPa. Note that the area of real contact is maximal at $d_K \approx 7$ nm, which corresponds to the point where there is just enough fluid to fill the space between the solids. This is illustrated in figure 11, which shows the wet (and dry) area as a function of the Kelvin length d_K . Note that for $d_K > 7$ nm the interface is filled with liquid. In this case the negative pressure $2\gamma/d_K$ will prevail (nearly) everywhere at the interface and the area of real contact will therefore be proportional to $1/d_K$, which is indeed the dependence of A/A_0 on d_K observed in figure 10 for $d_K > 7$ nm. In fact, we can accurately describe the behavior of the contact area for large and small d_K . Thus, when $d_K = 0$ no liquid occurs at the interface, and since the applied (squeezing) pressure p_0 is very small the area of real contact is linearly related to p_0 according to

$$\frac{A}{A_0} = \alpha p_0$$

where α can be calculated from the surface roughness power spectra and the effective elastic modulus as described elsewhere [23, 25]. We get $\alpha = 3.1 \times 10^{-10} \text{ Pa}^{-1}$, which gives the limit $A/A_0 \approx 1.24 \times 10^{-3}$ as $d_K \rightarrow 0$, in good agreement with figure 10.

In the opposite limit of large d_K (nearly) the whole interface is filled by fluid so that the effective pressure acting on the block is the sum of the applied pressure p_0 and the capillary pressure $2\gamma/d_K$, giving

$$\frac{A}{A_0} = \alpha \left(\frac{2\gamma}{d_K} + p_0 \right).$$

This relation (denoted ‘fully wet interface’) is shown in figure 10 and agrees very well with the numerical result for $d_K > 7$ nm.

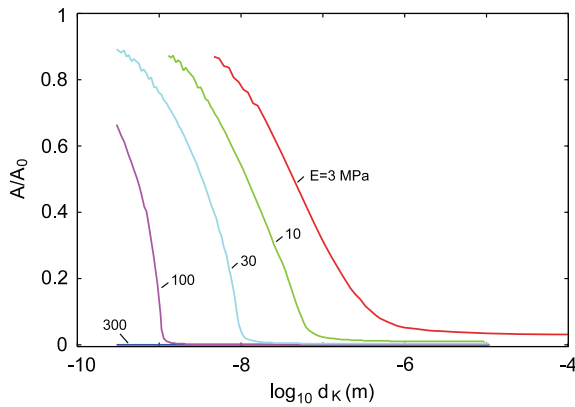


Figure 12. The area of real contact as a function of the logarithm of the Kelvin capillary width d_K . For a hard surface with the root-mean-square roughness $h_{rms} = 6 \mu\text{m}$ in contact with elastic solids (with flat surfaces) with the Poisson ratio 0.5 and several different Young moduli, $E = 3, 10, 30, 100$ and 300 MPa. The (nominal) squeezing pressure $p = 0.1$ MPa.

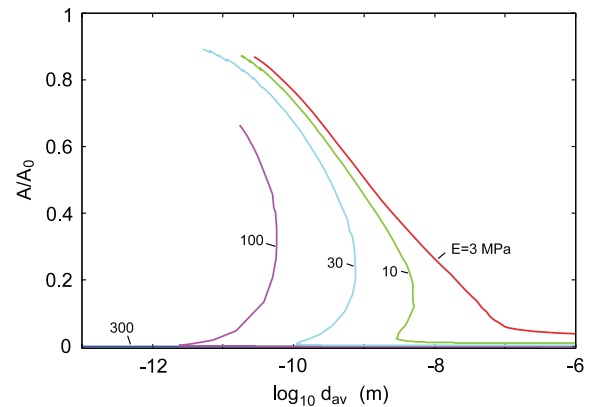


Figure 13. The area of real contact as a function of the logarithm of the average width, d_{av} , of the water layer between the surfaces. For a hard surface with the root-mean-square roughness $h_{rms} = 6 \mu\text{m}$ in contact with elastic solids with the Poisson ratio 0.5 and several different Young moduli, $E = 3, 10, 30, 100$ and 300 MPa. The (nominal) squeezing pressure $p = 0.1$ MPa.

3.2. Elastically soft solids

Consider the contact between an elastically soft solid with a flat surface and a hard, randomly rough, substrate with the power spectrum shown in figure 5, upper curve. This system exhibits more complex and interesting behavior than the case of elastically hard solids studied in the last section. Thus, we find that when the relative humidity decreases, resulting in a higher negative pressure in the capillary bridges, there may be a strong increase in the area of real contact because of elastic deformations of the solid walls, which are pulled into closer contact by the capillary adhesive forces. This is in sharp contrast to the case of hard solids (with relatively smooth surfaces) studied above, where the contact area was maximal when there was just enough liquid to fill the space between the (almost) undeformed solid walls.

Figure 12 shows the area of real contact as a function of the logarithm of the Kelvin capillary width d_K , for a hard surface with the root-mean-square roughness $h_{rms} = 6 \mu\text{m}$, in contact with elastic solids (with flat surfaces) with the Poisson ratio 0.5, and several different Young moduli, $E = 3, 10, 30, 100$ and 300 MPa. The (nominal) squeezing pressure $p = 0.1$ MPa. Note that for low enough RH (i.e. for small enough capillary distance d_K) the area of real contact increases rapidly with decreasing RH. This results from the strong capillary bridges pulling the solids into close contact. As expected, this effect start at higher and higher RH as the elastic modulus of the solids decreases. For the stiffest solid, $E = 300$ MPa, the area of real contact does not increase when the RH is reduced even to the point that the height of the fluid bridges is of molecular size $d_K \approx 0.5$ nm (below which the continuum theory fails).

Figure 13 shows again the area of real contact but now as a function of the logarithm of the average width, d_{av} , of the water layer between the surfaces. We define $d_{av} = V/A_0$, where V is the volume of water between the surfaces and A_0 the nominal (or projected) surface area. This figure illustrates an interesting effect: as the RH decreases, in some range of RH the amount of liquid between the surfaces increases as the RH decreases,

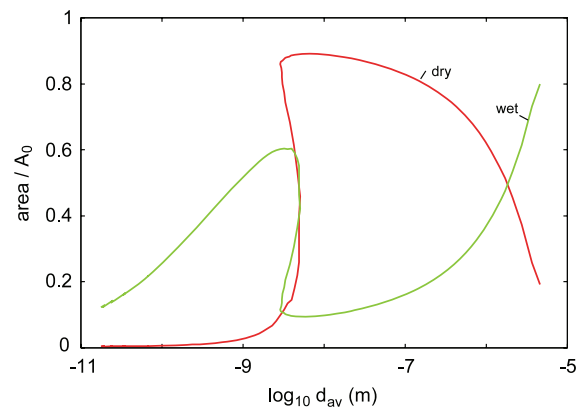


Figure 14. The dry and wet area as a function of the logarithm of the average width, d_{av} , of the water layer between the surfaces. For a hard surface with the root-mean-square roughness $h_{rms} = 6 \mu\text{m}$ in contact with elastic solids with the Poisson ratio 0.5 and the Young modulus $E = 10$ MPa. The (nominal) squeezing pressure $p = 0.1$ MPa.

i.e., water from the atmosphere condenses at the interfacial region between the solids. The reason for this is that when the RH decreases the surfaces are pulled together, which implies that the wet interfacial area (where $u(\mathbf{x}) < d_K$) increases, and this increase is so fast that the volume of liquid between the surfaces increases in spite of the fact that the capillary height decreases.

This effect is also illustrated in figure 14, which shows the wet (and dry) area as a function of the logarithm of the average width, d_{av} , of the water layer between the surfaces.

In figure 15 we show the stress as a function of the (average) interfacial separation \bar{u} , during pull-off. The area under the curves (for positive pull-off stress) determines the work of adhesion. Results are shown for elastic solids with flat surfaces, and with the Young's modulus $E = 3, 10$ and 100 MPa and the Poisson ratio $\nu = 0.5$. The results are for the Kelvin distance $d_K = 1 \mu\text{m}$ (corresponding to the relative humidity (RH) ≈ 0.999). Note that for the stiffest solid

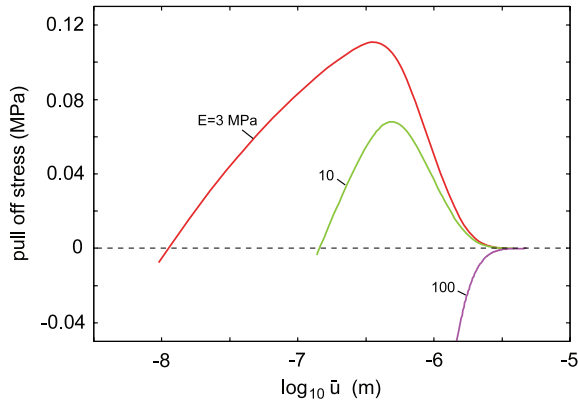


Figure 15. The stress as a function of the (average) separation \bar{u} during separation. The area under the curves (for positive pull-off stress) determines the work of adhesion. For a hard surface with the root-mean-square roughness $h_{\text{rms}} = 6 \mu\text{m}$ in contact with elastic solids (with the Young's modulus $E = 3, 10$ and 100 MPa and Poisson ratio $\nu = 0.5$) with flat surfaces. Results are shown for the Kelvin distance $d_K = 1 \mu\text{m}$ (corresponding to the relative humidity $\text{RH} \approx 0.999$).

$E = 100$ MPa the interaction is purely repulsive, i.e., the work of adhesion vanishes. For the elastically softer solids the work of adhesion is finite, but the pull-off stresses are much smaller than for the hard smooth surfaces studied in section 3.1, while the distances over which the pull-off force is non-negligible are much longer, both effects reflecting the much larger fluid film thickness (or Kelvin distance d_K) in the present case. The work of adhesion (i.e. the area under the curves in figure 15) for the $E = 3$ MPa case is $w = 0.11 \text{ J m}^{-3}$ and for the $E = 10$ MPa case we get $w = 0.062 \text{ J m}^{-3}$.

4. Applications

We present a few applications of the results presented above. Consider first rubber friction on a wet glass surface in the context of wiper blades. After rain or a car wash, the driver of a car does not immediately stop the motion of the wiper blades. In this case, as the water is removed by wiping and evaporation, as a function of time a high friction peak, with a friction considerably higher than the dry one, may be observed. This time period of enhanced friction is denoted as the *tacky regime*, and may prevail for several seconds. Experiments [33] have shown that in the tacky regime the attraction from water capillary bridges between the rubber and the glass substrate pull the rubber into close contact with the substrate so that the area of real contact is even larger in the tacky regime than for the perfectly dry contact. Since the applied pressure in the rubber–glass nominal contact area is very high in wiper blade applications, typically of the order of MPa, the additional contribution from the capillary bridges must be very large, of the order of MPa, in order to explain the strong increase (typically by a factor of two) in the friction. This implies that the height of the capillary bridges $d < 100$ nm. This also implies that the wiper blade glass–rubber friction may be considerably enhanced in humid conditions, where capillary bridges are formed spontaneously.

The high friction in the tacky region can block a wiper system. Capillary adhesion can be reduced by surface treatment of the rubber. Thus, halogenation results in a rubber surface layer which is elastically much stiffer than the bulk (by up to a factor of 100, see [34]) and will strongly reduce the friction coefficient in the tacky region, e.g. from 3 (no halogenation) to 1 (at 15% halogeneous concentration in the surface region) [35]. The surfaces of wiper blades are almost always exposed to halogenation. However, after a long time of use this layer of modified rubber may be removed by wear. Thus, the friction coefficient for very worn-out blades may exceed 3.

Capillary bridges may also give rise to strongly enhanced friction for lubricated rubber applications, if the lubrication film is very thin everywhere (e.g. even at the boundary of the nominal contact area). Thus, in a recent experiment [36], a rubber block was slid on a smooth steel surface lubricated by a drop of oil. In this case the oil film was everywhere very thin $d \approx 300$ nm, and the rubber–steel surface friction was observed to increase from ~ 1 to ~ 3 when the oil drop was added to the metal surface. In this experiment the applied nominal pressure was rather small, about 0.01 MPa. The capillary adhesive force can be estimated using $2\gamma/d \approx 0.3$ MPa, where we used $\gamma \approx 0.05 \text{ J m}^{-2}$. This is much larger than the applied nominal squeezing pressure, but because of the finite sliding speed (0.1 m s^{-1}) one cannot assume that all the fluid gets completely squeezed out from the asperity contact regions [37], and therefore the increase in the sliding friction will be smaller than indicated by the increase in the effective normal load.

Capillary adhesion is very important in biological adhesive systems used for locomotion. This has been studied in detail for tree frogs [4, 5] and stick insects [38]. These animals use smooth adhesive pads which are built from non-compact materials and are elastically very soft. To adhere to surfaces the animals inject a wetting liquid into the contact area. Experiments for stick insects have shown that the nominal frictional shear stress for sliding against smooth glass surfaces increases when the fluid film thickness decreases, e.g. during sliding long distances. During repeated sliding on the same surface area, the friction decreases continuously as more liquid accumulates on the surface—typically the frictional shear stress dropped from 0.15 to 0.05 MPa as the film thickness increased. Nevertheless, as expected, the nominal pad–substrate surface contact area did not change much since the work of adhesion (which determines the contribution to the contact area from the adhesional interaction) may be nearly constant (equal to 2γ) if enough liquid occurs at the interface, as indeed expected in the present case (note: the insects usually need to move on surfaces much rougher than the glass surface and must therefore inject much more liquid at the pad–substrate contact area than is necessary for the smooth glass surface). The pull-off force from the glass surface was nevertheless observed to increase when the film thickness decreased during repeated contact and pull-off. This is most likely a viscosity effect: during separation of two closely spaced solids separated by a thin fluid layer, fluid must flow towards the center of the contact area, and during ‘fast’ pull-off

this generates a strong negative pressure (effective adhesion) in the fluid because of viscous dissipation in the fluid. In this case, the thinner the fluid film the larger the peak force will be, as seen in the experiments.

As a final application of the theory presented above, let us consider the contact between the toe pad of a tree frog and a smooth glass plate. This system has been studied in great detail in [4]. At the toe pad–substrate interface occurs a wetting liquid, which is likely to be of the order of $\sim 1 \mu\text{m}$ thick at the edges of the toe pad–substrate contact regions (see [5]). Thus, the negative capillary pressure $2\gamma/d \approx 0.1 \text{ MPa}$. Because of the low effective elastic modulus of the toe pad, it deforms elastically so that a large fraction (about 50%) of the toe pad comes into close contact (less than 5 nm) with the glass surface, in spite of the fact that the natural height fluctuations of the toe pad surface (on the length scale of $\sim 10 \mu\text{m}$) are of the order of $\sim 1 \mu\text{m}$. The area of real contact manifests itself experimentally as a finite static friction force.

5. Discussion

The theory presented in section 2 is a mean-field type of theory, where the adhesive force F_a from the capillary bridges is taken into account by adding an adhesive pressure $p_a = F_a/A_0$ to the external squeezing pressure $p_0 = F_0/A_0$ acting on the block (F_0 is the normal load, which is assumed to act uniformly on the top surface of the block). This is likely to be an accurate approximation as long as a large fraction of the non-contact interfacial region is filled with liquid, e.g. for high relative humidity. However, for very low relative humidity and for large surface roughness, liquid bridges may only occur close to the outer edges of the asperity contact regions. If the regions occupied by fluid are very small compared to the diameter of the contact and non-contact regions, then we can consider the fluid filled regions as crack-tip process zones, and this limit can be studied using the adhesion theory developed elsewhere [24, 39]. In this theory the interface is studied at different magnifications, and an effective interfacial binding energy (per unit area), $\gamma_{\text{eff}}(\zeta)$, is introduced. If one assumes that the continuum theory of capillary forces is still valid for the small capillary bridges which occur at low RH then $\gamma_{\text{eff}}(\zeta_1) = 2\gamma \cos \theta$. However, most likely the continuum theory is not valid for narrow (molecular sized) capillary bridges, and one may have to treat $\gamma_{\text{eff}}(\zeta_1) = \Delta\gamma$ as an empirical parameter to be determined directly from experimental data.

In the theory developed in section 2 we always assumed thermal equilibrium. However, it is known that the formation of capillary bridges in a humid atmosphere is a thermally activated process, with a continuum of activation energies and hence relaxation times. Thus, in general it may take a very long time to reach (or come close to) thermal equilibrium. In the study by Maarten [31] for microcantilevers, at the relative humidity 0.3, the average crack length (defined as the non-contact part of the cantilever) decreased with increasing times from $\approx 700 \mu\text{m}$ initially to $\approx 550 \mu\text{m}$ after 2.5 h, to $\approx 400 \mu\text{m}$ after 5 h, and to $\approx 375 \mu\text{m}$ after 10 h. After this time no further decrease of the crack length was observed. In general, the increase in adhesion and friction with increasing time, as

a result of thermally activated formation of capillary bridges, has been studied in detail, and is of great importance in many systems of fundamental or applied interest [40–42].

Another limitation of the theory presented in section 2 is that it is only valid if most of the relevant repulsive wall–wall interaction occurs for separations \bar{u} that are small enough that, for the actual physical system, there are enough asperity contact regions (to obtain enough self-averaging) that the analytical theory can be applied. That is, the analytical contact mechanics theory is for an infinite system (thermodynamic limit), and for a randomly rough surface (with a Gaussian probability height distribution) there will always be infinitely high asperities, and contact between two solids will occur for any (average) separation \bar{u} between the solids. In fact, for large \bar{u} we have the exact result $p \sim \exp(-\alpha\bar{u}/h_{\text{rms}})$, which shows that a repulsive pressure p will act between the solids for arbitrary large separation \bar{u} . However, for finite-sized systems, the highest asperities have a finite height, which for macroscopic systems typically is of the order of $\sim 10h_{\text{rms}}$ (see appendix A in [23]), but in the context of MEMS may be much smaller due to their small physical size. In fact, de Boer has estimated the highest asperities in the crack-tip process zone to be only $\approx 3.7h_{\text{rms}}$. It is clear that the analytical theory is only valid if the important repulsive contribution to the work of adhesion occurs for separations $\bar{u} < 3.7h_{\text{rms}}$. In our applications to microcantilever adhesion most of the relevant repulsive interaction occurs for $\bar{u} < 3.2h_{\text{rms}}$ so the theory is likely to be at least semiquantitatively correct.

In the GW theory a similar problem is related to the height of the highest asperities, but in addition the exact form of the tail of the height distribution for large separation matters a lot for the contact mechanics and in particular for the relation between \bar{u} and p . However, this is an artifact of the GW theory, and when the long-range elastic coupling is taken into account, as in the theory of Persson, the contact mechanics becomes much less dependent on the details of the height distribution. This has been verified by finite element method calculations [19] for polymer surfaces [16] where, in spite of the fact that the height probability is rather non-Gaussian for large asperity heights (see figure 14 in [17]), the contact mechanics obeys the usual behavior with the area of real contact proportional to the load and the average interfacial separation depending on the squeezing pressure as $p \sim \exp(-\alpha\bar{u}/h_{\text{rms}})$, in good numerical agreement with the Persson theory [17]. This can be explained by the fact that, because of long-range elastic deformation, not only the asperities close to the top of the Gaussian distribution will make contact, but a larger range of asperity heights will be involved (which is the reason why the asymptotic relation $p \sim \exp(-\alpha\bar{u}/h_{\text{rms}})$ is exponential rather than Gaussian (reflecting a Gaussian height distribution) $p \sim \exp[-b(\bar{u}/h_{\text{rms}})^2]$ as in the GW theory). This is illustrated in figure 16 for a situation where this fact is particularly clear.

The analytical theory presented in section 2 for the limiting case of an interface completely filled with fluid (e.g. high relative humidity) indicates that the most important property of the rough surface is the root-mean-square roughness h_{rms} , while other properties such as (for self-affine

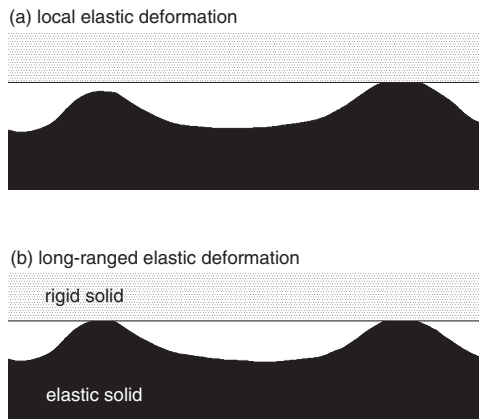


Figure 16. (a) In the Greenwood–Williamson (GW) contact mechanics model only local (asperity) elastic deformations are included. (b) In reality the elastic deformation is long ranged, and asperities which never could be in contact in the GW theory because they are too low could be in contact when the elastic deformation is fully included in the analysis. For this reason the GW theory is much more sensitive to the exact form of the probability distribution of asperity heights for large asperity height than in a more accurate analysis which includes the long-range elastic deformations.

fractal surfaces) the fractal dimension D_f and the upper and lower cut-off wavevectors q_1 and q_0 are much less important because the parameter α in the relation $p \sim \exp(-\alpha \bar{u}/h_{\text{rms}})$ is very insensitive to these quantities [18]. This is also likely to be the case for non-fractal surfaces. This fact is consistent with experiments of van Zwol *et al* [32], who observed that surfaces with very different q_0 but the same root-mean-square roughness $h_{\text{rms}} \approx 1.5$ nm exhibited the same capillary adhesion. We conclude that the rms roughness gives the predominant effect on the adhesive force due to capillary bridges.

In the theory presented in section 2 we have neglected plastic deformation of the solids and the disjoining pressure due to adsorbed (water) layers. The problem of the influence of plastic yielding on the contact mechanics was studied in [29], where it was found to have a very small influence on the capillary adhesion. I have analyzed the same problem using the more accurate contact mechanics theory I have developed. I find that the surface roughness with wavelength longer than $\sim 0.2 \mu\text{m}$ undergoes negligible plastic deformation, while some plastic deformation occurs for roughness at shorter length scales. Plastic deformation will tend to smoothen the surfaces and hence reduce the stored elastic energy. This in turn will enhance the capillary adhesion. I will report on this study elsewhere.

The presence of adsorbed water layers on the hydrophilic polysilicon surfaces used in the experiment [29] will also play a role in the capillary adhesion process. Unfortunately, a water adsorption isotherm does not currently exist for polysilicon surfaces, which makes it impossible to definitively determine the role of adsorbed water layers on the capillary adhesion problem. However, the fact that we obtained good agreement with experiment neglecting this effect for high relative humidity indicates that it may not be very important

(for $\text{RH} > 0.9$) for the microcantilever applications discussed above.

6. Summary and conclusion

I present a general theory for how the contact area and the work of adhesion between two elastic solids with randomly rough surfaces depends on the relative humidity. The surfaces are assumed to be hydrophilic, and capillary bridges form at the interface between the solids. For elastically hard solids with relatively smooth surfaces, the area of real contact and therefore also the sliding friction are maximal when there is just enough liquid to fill out the interfacial space between the solids, which typically occurs for $h_K \approx 3h_{\text{rms}}$, where h_K is the height of the capillary bridge and h_{rms} the root-mean-square roughness of the (combined) surface roughness profile. For elastically soft solids, the area of real contact is maximal for very low humidity where the capillary bridges are able to pull the solids into nearly complete contact. In both cases, the work of adhesion is maximal (and equal to $2\gamma \cos \theta$, where γ is the liquid surface tension and θ the liquid–solid contact angle) when $d_K \gg h_{\text{rms}}$, corresponding to high relative humidity.

The theory is compared to experimental data for microcantilever structures. The theory is in good agreement with the data while the classical Greenwood–Williamson theory fails qualitatively. I also present applications to rubber wiper blades, where the theory can explain the large friction observed in the so called ‘tacky region’ for nearly dry contacts, where the capillary bridges pull the rubber into intimate contact with the glass substrate over a large fraction of the nominal contact area.

References

- [1] Israelachvili J 1992 *Intermolecular and Surface Forces* (New York: Academic)
- [2] Bocquet L, Charlaix E, Cilibetro S and Crassous J 1998 *Nature* **396** 735
- [3] Halsey T C and Levine A J 1998 *Phys. Rev. Lett.* **80** 3141
- [4] Creton C and Gorb S (ed) 2007 *MRS Bull.* **32** 467–508 (articles on bioadhesion)
- [5] Federle W, Barnes W J P, Baumgartner W, Drechsler P and Smith J M 2006 *J. R. Soc. Interfaces* **3** 689
- [6] Persson B N J 2007 *J. Phys.: Condens. Matter* **19** 376110
- [7] Mate C M 1992 *J. Appl. Phys.* **72** 3084
- [8] Mastrangelo C H and Hsu C H 1993 *J. Microelectromech. Syst.* **2** 33
- [9] Mastrangelo C H and Hsu C H 1993 *J. Microelectromech. Syst.* **2** 44
- [10] Greenwood J A and Williamson J B P 1966 *Proc. R. Soc. A* **295** 300
- [11] Carbone G and Bottiglione F 2008 *J. Mech. Phys. Solids* doi:10.1016/j.jmps.2008.03.011
- [12] Persson B N J, Sivebaek I M, Samoilov V N, Zhao K, Volokitin A I and Zhang Z 2008 to be published
- [13] Bush A W, Gibson R D and Thomas T R 1975 *Wear* **35** 87
- [14] Borri-Brunetto M, Chiaia B and Ciavarella M 2001 *Comput. Methods Appl. Mech. Eng.* **190** 6053
- [15] Hyun S, Pei L, Molinari J F and Robbins M O 2004 *Phys. Rev. B* **70** 026117
- [16] Yang C, Tartaglino U and Persson B N J 2006 *Eur. Phys. J. E* **19** 47

- [15] Campana C and Müser M H 2007 *Europhys. Lett.* **77** 38005
- [16] Benz M, Rosenberg K J, Kramer E J and Israelachvili J N 2006 *J. Chem. Phys.* **110** 11884
- [17] Yang C and Persson B N J 2008 *J. Phys.: Condens. Matter* **20** 215214
- [18] Persson B N J 2007 *Phys. Rev. Lett.* **99** 125502
- [19] Pei L, Hyun S, Molinari J F and Robbins M O 2005 *J. Mech. Phys. Solids* **53** 2385
- [20] Samoilov V N, Sivebaek I M and Persson B N J 2004 *J. Chem. Phys.* **121** 9639
- [21] Yang C, Tartaglino U and Persson B N J 2006 *J. Phys.: Condens. Matter* **18** 11521
- [22] Johnson K L 1985 *Contact Mechanics* (Cambridge: Cambridge University Press)
- [23] Persson B N J 2006 *Surf. Sci. Rep.* **61** 201
- [24] Persson B N J 2002 *Eur. Phys. J. E* **8** 385
- [25] Persson B N J 2001 *J. Chem. Phys.* **115** 3840
- [26] Persson B N J, Bucher F and Chiaia B 2002 *Phys. Rev. B* **65** 184106
- [27] de Boer M P 2006 private communication
- [28] See, e.g., Persson B N J, Albohr O, Tartaglino U, Volokitin A I and Tosatti E 2005 *J. Phys.: Condens. Matter* **17** R1
- [29] DelRio F W, Dunn M L and de Boer M P 2008 *Scr. Mater.* doi:10.1016/j.scriptamat.2008.02.037
- [30] DelRio F W, Dunn M L, Phinney L M, Bourdon C J and de Boer M P 2007 *Appl. Phys. Lett.* **90** 163104
- [31] de Boer M P 2007 *Exp. Mech.* **47** 171
- [32] van Zwol P J, Palasantzas G and De Hosson J Th M 2007 *Appl. Phys. Lett.* **91** 101905
- [33] Deleau F, Mazuyer D and Koenen A 2008 *Tribol. Int.* at press
- [34] Koenen A 2008 private communication
- [35] Koenen A and Sanon A 2007 *Tribol. Int.* **40** 1484
- [36] Wangenheim M and Kröger M 2008 *Proc. of the 9th Biennial ASME Conf. on Eng. Systems Design and Analysis (Haifa, July 2008)* ESDA2008-59S07
- [37] Persson B N J and Mugele F 2004 *J. Phys.: Condens. Matter* **16** R295
- [38] Drechsler P and Federle W 2006 *J. Comp. Physiol. A* **192** 1213
- [39] Peressadko A G, Hosoda N and Persson B N J 2005 *Phys. Rev. Lett.* **95** 124301
- [40] Bocquet L, Charlaix E, Ciliberto S and Crassous J 1998 *Nature* **396** 735
- [41] Riedo E, Levy F and Braun H 2002 *Phys. Rev. Lett.* **88** 185505
Riedo E, Palaci I, Boragno C and Brune H 2004 *J. Phys. Chem. B* **108** 5324
- [42] Persson B N J 2000 *Sliding Friction: Physical Principles and Applications* 2nd edn (Heidelberg: Springer)